Astronomy & Astrophysics manuscript no. output
October 11, 2021

An asteroseismic expedition for the missing physics in stellar evolution

Non-linear inversion for stellar structure

A. Le Saux[1], E. P. Bellinger[2,3], S. Basu[4], and W. H. Ball[5,3]

[1] University of Exeter, Physics & Astronomy, EX4 4QL Exeter, UK; e-mail: al598@exeter.ac.uk
[2] Max Planck Institute for Astrophysics, Garching, Germany
[3] Stellar Astrophysics Centre, Department of Physics and Astronomy, Aarhus University, Denmark
[4] Department of Astronomy, Yale University, P.O. Box 208101, New Haven, CT 06520-8101, USA
[5] School of Physics & Astronomy, University of Birmingham, Edgbaston, Birmingham B15 2TT, UK

October 11, 2021

ABSTRACT

Context. To investigate internal stellar structure, inversion techniques have been developed in the past decades. These methods use helio- and asteroseismology to constrain and build models of stars. Here we present a new approach to infer stellar structure through inversion.
Aims. To date, most methods used to perform inversions are linear. This can introduce errors, particularly for evolved stars. Thus we propose here a method based on non-linear inversion.
Methods. The inversions methods are based on the stellar structure equations. Here we propose to build static stellar models with a flexible composition profile and to use a stellar evolution code to relax these models, i.e. to solve the full non-linear equations of stellar structure. The composition profiles that are compatible with the stellar oscillation data are sought using a Markov chain Monte Carlo (MCMC) method.
Results. Our results show that we can indeed obtain a realistic stellar structure using a non-linear inversion. We first apply it to the Sun and compare the results with those from linear inversion methods. We then apply it to two of the best solar-type stars observed by the *Kepler* mission, 16 Cyg A & B.

Key words. stars: evolution – stars: interiors – asteroseismology

1. Introduction

Stellar evolution is the science that deals with the life of stars, trying to understand how they are formed, how they disappear and all their major evolutionary stages. In addition to being interesting in its own right, stellar evolution is important not only for stellar physics but also throughout astronomy. For example, constraining planet-host stars aids exoplanetary science, and precisely determining stellar ages is essential for studying the evolution of the galaxy. At smaller scales, it also allows to predict the future of our Sun, and its interaction with the Earth.

Although stellar evolution theory is widely used and generally accepted, we know that it is still missing some physics. In the solar case, it has been highlighted that the standard models of the Sun are highly significantly discrepant with the helioseismic observations of the Sun (see for examples Basu 2016; Christensen-Dalsgaard 2021). For examples, there is still some unexplained discrepancies between the helioseismic sound speed profile and the model one (). It has also been shown that diffusion and gravitational settling of all elements heavier that hydrogen play a very important role when building solar models (Christensen-Dalsgaard et al. 1993; Basu 2016).

In this project, we will focus on stellar structure by trying to obtain better constraints on stellar interiors using stellar oscillation data. Asteroseismology is the science that studies the modes of stellar oscillation to probe the internal structure and dynamics of stars. It is a powerful tool to study stellar interiors that are otherwise inaccessible to direct observation.

Although stellar evolution theory is widely used and generally accepted, we know that it is still missing some physics. In the solar case, it has been highlighted thanks to helioseismology—the study of solar oscillations—that the standard models of the Sun are highly significantly discrepant with the observational data of the Sun (see for examples Basu 2016; Christensen-Dalsgaard 2021). For example, there are still some unexplained discrepancies between the helioseismic sound speed profile and the theoretical one (). It has also been shown that diffusion and gravitational settling of all elements heavier that hydrogen play a very important role when building solar models (Christensen-Dalsgaard et al. 1993; Basu 2016). These results were obtained thanks to helioseismic structure inversion methods, which consist in inferring a internal structure of the Sun using the observed frequencies of its modes of oscillation. These methods have been proven powerful as they give deep insight into the solar interior.

With the arrival of CoRoT in 2006 (Auvergne et al. 2009) and *Kepler* in 2009 (Borucki et al. 2010), asteroseismology underwent a revolution thanks to the precision of their observations, allowing to probe the interior of stars other than the Sun. Moreover, these observations are increasing thanks to NASA's TESS satellite (Ricker et al. 2014), which has been operating since April 2018, and the arrival of PLATO, an ESA project,

Table 1. Characteristics of the Sun (from MESA).

Variables	Sun
Age (Gyr)	4.59
M (g)	$1.98840987 \times 10^{33}$
R (cm)	6.957×10^{10}
L (erg.s^{-1})	3.828×10^{33}
[Z/X]	0.02293
$T_{\rm eff}$ (K)	5772.0

which is scheduled for the end of 2026 (Rauer et al. 2014). These satellites have already provided data on hundreds of thousands of stars, and millions more are expected in the coming years. The diversity of the observed stars offer a unique laboratory to determine precisely stellar structure of a wide variety of stars. Indeed, we are no longer limited to one star but now have access to many stars at almost every step of stellar evolution. This presents an opportunity to really test stellar evolution theory.

2. Models & Data

2.1. Sun

As the Sun is the best known star, we have chosen to start with an analysis of this star. This allows for precise comparison not only with observations but with previous studies that used different methods to get similar results (e.g., linear inversion techniques).

2.1.1. Observational data

The main characteristics of Sun are those used in the MESA stellar evolution code (Paxton et al. 2011, 2013, 2015, 2018, 2019). They are presented in Table 1. The age is from Bahcall et al. (2005), mass M, radii R, luminosity L and effective temperature $T_{\rm eff}$ from the *IAU 2015 Resolution B3*, and the metallicity from Grevesse & Sauval (1998). Hereinafter all variables with a subscript $\odot$ will refer to the values introduced in Table 1.

The observational oscillations frequencies for the Sun used in this project are from the Birmingham Solar Oscillations Network (BiSON) (Broomhall et al. 2009; Davies et al. 2014; Hale et al. 2016).

2.1.2. Model

For this project we are using the MESA stellar evolution code. The initial solar model used has been calibrated using the *solar_simplex_calibration* test suite of the MESA code. This test suit allows to calibrate a 1 $M_\odot$ in order to get an Standard Solar Model (SSM) (Serenelli 2016). Hereinafter this model is called the Initial Calibrated Solar Model (ICSM).

The calibration process uses the following variables: the mixing length parameter $\alpha_{\rm MLT}$, and the initial value of the abundances of helium, Y_0, and heavy elements, Z_0. We incorporate also the settling and diffusion of elements during the evolutionary calculations. These variables are adjusted until the radius R, luminosity L, relative abundance of metals $[Z/X]$, effective temperature $T_{\rm eff}$, age, and the sound speed profile $c_{\rm s}(r)$, of the model are as close as possible to the observed solar values. We recall that relative abundances are defined as

$$[Z/X] = \log(Z/X)_{\rm star} - \log(Z/X)_\odot \quad (1)$$

with $(Z/X)_\odot$ the relative abundance of metals of the Sun.

Table 2. Characteristics of our ICSM.

Variables	ICSM
$Age^{(a)}$ (Gyr)	4.610
M ($M_\odot$)	1.000000000000
R ($R_\odot$)	1.000001647540
L ($L_\odot$)	0.999999989931
[Z/X](dex)	0.02293
$T_{\rm eff}$ (K)	5771.99865977

Notes. $^{(a)}$ Age take into account the pre-ZAMS period.

Table 3. Characteristics of 16 Cyg A & B (from Bellinger et al. 2017).

Variables	16 Cyg A	16 Cyg B
Age (Gyr)	6.90 ± 0.40	6.80 ± 0.28
M ($M_\odot$)	1.080 ± .016	1.030 ± 0.15
R ($R_\odot$)	1.22 ± 0.02	1.12 ± 0.02
L ($L_\odot$)	1.56 ± 0.05	1.27 ± 0.04
[Fe/H] (dex)	0.096 ± 0.0026	0.052 ± 0.021

The characteristics of the model resulting from the calibration are presented in Table 2.

2.2. 16 Cyg A & B

In a second part, we propose to study and test our method on two solar-like stars observed by *Kepler*, KIC 2069424–12069449, also known as 16 Cyg A and 16 Cyg B. These stars form part of the triple system of 16 Cygni and are two of the best stars from *Kepler* data. Results obtained for these two solar analogs can then be compared with the work of Bellinger et al. (2017) who use linear inversion techniques to study their internal structure.

2.2.1. Observational data

The main characteristics of these two stars are presented in Table 3. Radii R and luminosity L are from White et al. (2013), ages and masses, M are from Bellinger et al. (2016) and metallicities from Ramírez et al. (2009).

The observational oscillations frequencies for 16 Cyg A and B used in this project are from the Davies et al. (2015). Their values are given in Appendix **??**.

2.2.2. Model

The two initial models used for 16 Cyg A and 16 Cyg B are the GOE models from Silva Aguirre et al. (2017).

3. Methodology

3.1. Inversion of oscillation frequencies

The frequencies of oscillations modes of a star are set by its internal structure. It is therefore possible to constrain the internal stellar structure through an inverse analysis of the observations of these modes. In order to get information on stellar structure from oscillations frequencies, one needs to start by perturbing the equations of motions. Then assuming that the time dependence of a perturbation is of the form $e^{-i\omega t}$ and considering adiabatic oscillations we have (Basu 2016):

$$-\omega^2 \rho \boldsymbol{\xi} = -\nabla P_1 + \rho \boldsymbol{g_1} + \rho_1 \boldsymbol{g} \quad (2)$$

with ω the oscillation frequency, ρ the density, $\boldsymbol{\xi}$ the displacement vector associated with the oscillations, P the pressure and $\boldsymbol{g}$ the acceleration of gravity. The subscript 1 corresponds to the Eulerian perturbation of a quantity. Eq. (2) gives insight into the analytical link between oscillation frequencies and stellar structure. It is clear that these frequencies rely on the spatial dependence of density, pressure and gravity. This equation is the basis of the linear inversion technique.

As mentioned earlier, in order to perform this inverse analysis, the equations of motions are perturbed and then linearised. Bellinger et al. (2020, 2021) pointed out that this method could introduce errors. Indeed, the linear regime approximation is not always perfectly justified, particularly for evolved stars. Moreover, this also requires a manual adjustment for numerous free parameters. This motivates us to study and develop a non-linear inversion technique.

3.2. Correcting modeled frequencies

Modelling the near surface layers of a star is still a real challenge. First of all, in stellar atmospheres the diffusion approximation does not hold anymore for the radiative transport of energy, so one need to solve the full radiative-transfer equations. Secondly, convection is still a major problem in the near surface layers, but it also brings some additional issues: it is inefficient, so it can not be considered adiabatic anymore; and its interaction with the atmosphere is very complex. Also, magnetic fields play an important role in the atmosphere, in particular in the heating of the chromosphere or in the development of several instabilities such as waves and flares. Finally, opacities at low temperatures can be quite uncertain.

All of this is not taken into account in stellar evolutionary modelling. Most of the time, a simplified model of atmosphere is used, such as an Eddington-τ relation for a gray atmosphere. Consequently, modelled frequencies are not directly comparable with observed ones. This is known as the surface term problem. As explained in Basu (2016), this introduces a frequency shift that depends mostly on frequency and is independent of spherical degree. However, the surface effects are not the only source of discrepancies between the Sun and standard solar models.

In order to compensate for this frequency shift, several methods have been developed (Roxburgh & Vorontsov 2003; Kjeldsen et al. 2008; Gruberbauer et al. 2012). Because it has been shown to be the (so far) favorable treatment of the surface term (Schmitt & Basu 2015; Ong et al. 2021), we work with the method described in Ball & Gizon (2014). It suggests to add to the modelled frequencies the following parametrization

$$\delta\nu = \left(a_{-1}(\nu/\nu_{\rm ac})^{-1} + a_3(\nu/\nu_{\rm ac})^3\right)/\mathcal{I} \tag{3}$$

with a_{-1} and a_3 being coefficients that are fit for a given stellar model (hence the dependence of the frequency shift on the model), $\nu_{\rm ac}$ is the acoustic cut-off frequency, and $\mathcal{I}$ is the normalized mode inertia. For a given star, the acoustic cut-off frequency is defined using the scaling relation

$$\frac{\nu_{\rm ac}}{\nu_{\rm ac,\odot}} = \frac{g}{g_\odot}\left(\frac{T_{\rm eff}}{T_{\rm eff,\odot}}\right)^{-1/2} \tag{4}$$

with $T_{\rm eff}$ the effective temperature and the subscript $\odot$ indicating the solar value.

However, even if this surface term correction allows a better agreement between observations and models, it is known that the differences between the sun and the standard solar model don't solely belong to the surface effects. This indeed suggests that the theroy of stellar evolution and structure misses, or inaccurately model, some physics.

3.3. Flexible representation of a composition profile

In MESA, a snapshot of the composition profile is set with the radial evolution of 3 variables: X, Y and Z. The elements contained in Z depend on which network is chosen. In this work, we are using two different networks: 'basic.net' and 'pp_cno_extras.net'. The former contains only 8 species (^{1}H, ^{3}He, ^{4}He, ^{12}C, ^{14}N, ^{16}O, ^{20}Ne, ^{24}Mg) and the latter 25 (the previous 8 + ^{2}H, ^{7}Li, ^{7}Be, ^{8}B, ^{13}C, ^{13}N, ^{13}N, ^{14}O, ^{15}O, ^{17}O, ^{18}O, ^{17}F, ^{18}F, ^{19}F, ^{18}Ne, ^{19}Ne, ^{22}Mg). Using one or the other depends on the information we have on the star we aim to model. Particularly, stars more massive than the Sun and stars at later phases of evolution need more detailed nuclear networks. The relative abundance of each element is taken from the solar photospheric composition as determined by either Grevesse & Sauval (1998) or Asplund et al. (2009). As we know we have the constraint X+Y+Z=1, we only need to parametrize 2 of the 3 variables. X is always a variable because we need to ensure that the X profile is strictly increasing from the centre toward the surface, then we can either chose Y or Z as the second independent variable.

In the MESA models used here, the composition profile is discretized in 1500–2000 points. This is too much if we want to parametrize the profile. Indeed, in our method we would like to build a model with a structure that allows to get oscillations frequencies as close as possible to the observational data. If we keep these 1500–2000 points for the composition profile, it means that the algorithm will need to work with as much input parameters. This is way to much to get results in a reasonable amout of time. Consequently, in order to reduce this dimensionality, we use a P-splines representation of the composition profile. P-splines, or Penalized B-splines, were developed by Eilers & Marx (1996). The concept is based on B-splines but with addition of a parameter to control the smoothness of the representation. This smoothness parameter, λ, is optimized using the equation:

$$Q = \sum_i (o_i - b_i)^2 + \lambda \sum_i (b_i - b_{i-1})^2 \tag{5}$$

where o_i is the original value of X, Y or Z at given point in radius and b_i is the build value from the P-splines method. The main advantage of the technique is that it allows to obtain a faithful representation of the composition profile with only a limited number of parameters. These parameters, called knots, will be regularly spaced in term of acoustic depth, which is defined as (Gough 1990)

$$\tau(r) = \int_r^{R_\star} \frac{{\rm d}r}{c} \tag{6}$$

with $R_\star$ being the total radius of the star. Indeed, it is assumed that no information travel faster than the sound speed. We determined the optimal number of knots as 65 by analyzing the convergence of the cumulative error on the rebuild profile compare to the initial, as presented on Fig. 1. This value was already used by Basu et al (?). The position of the knots are showed on Fig. 2.

Finally, we parametrize the perturbation to the composition profile, δA, instead of the composition profile itself, A. Then the new profile will be $A' = A + \delta A$, with $A = X$, Yor Z. This is to avoid any problem with discontinuities, particularly the one at the convective-radiative boundary.

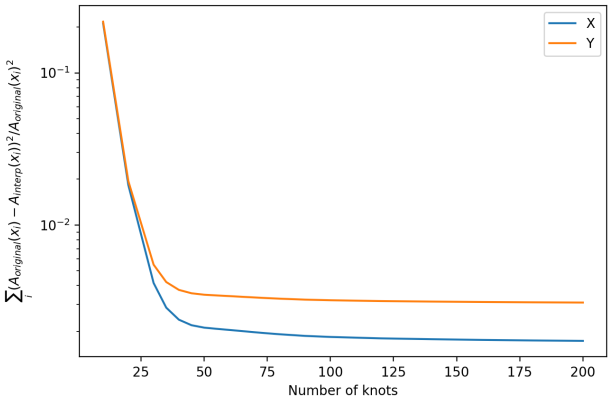

Fig. 1. Evolution of the relative squared error on the composition profile build from P-splines methods compare to the original one, as a function of number of knots.

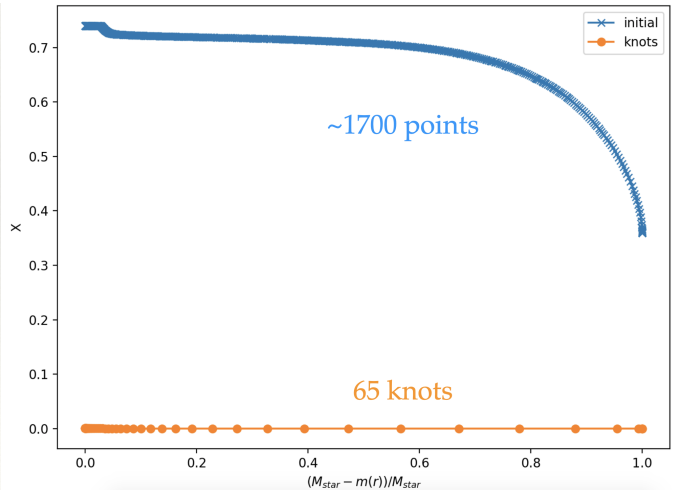

Fig. 2. Evolution of the X profile as provided in a MESA model of the Sun and the corresponding position of the knots used for the P-splines representation.

3.4. MCMC

Now that we are able to build flexible static models of stars and compare them to asteroseismological data, the next step is to determine which structure allows the best fit to these observations. This step will be automated using Markov Chain Monte Carlo (MCMC). This method allows the exploration of the parameter space with the objective to sample from the posterior distribution. (see e.g. Brooks et al. (2011) for review on MCMC). Here we work with python package *emcee* (Foreman-Mackey et al. 2013). The parameters used are the mixing length parameter $\alpha_{\rm MLT}$ and the knots of the X and Y (or Z) composition profiles. There are 65 knots per profile with 40 that are located in the convection zone. As mixing within the convection zone is efficient, we can consider that the relaxation step will homogenize the composition in the whole region, and therefore there will always be a flat composition profile in the convective zone. With this assumption the number of parameters is reduced from 65 to 25 per profile. So, in the end the MCMC will work with 51 parameters.

These parameters are the input of a function p which return a density of probability for a given combination of parameters. The objective of the MCMC is to maximize this function, which we define using χ^2 function:

$$p(\alpha_{\rm MLT}, X_1, \ldots, X_N, Y_1, \ldots, Y_N) = -\log(\chi^2). \quad (7)$$

The χ^2 function is defined as

$$\chi^2 = \sum_j \frac{(O_j - M_j)^2}{\sigma_j^2}, \quad (8)$$

with the O_j and M_j that are respectively the observed and modelled values of oscillations frequencies ν_i, radius R, luminosity L, and metal abundance at the surface [Fe/H]. Variables σ_j are the uncertainties on the observed values.

4. Results

4.1. Relaxation step

First, it is important to study the influence this step could have on the results. The relaxation is performed by MESA using the *relax_initial_composition* function. Here we extract the composition of the ICSM, parametrize it with B-splines and rebuild a composition profile without adding any perturbation to it. Then we relax the model over a few time steps. As we can see on Fig. 3 and 4 for the hydrogen and sound speed profile respectively, this step can introduce some perturbations.

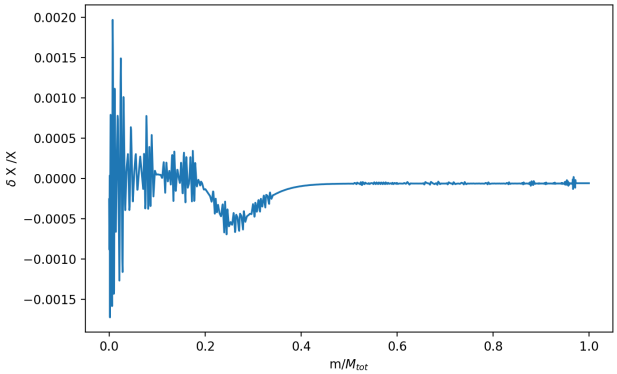

Fig. 3. Evolution of the X profile relative difference between the ICSM and a relaxed model with the same composition.

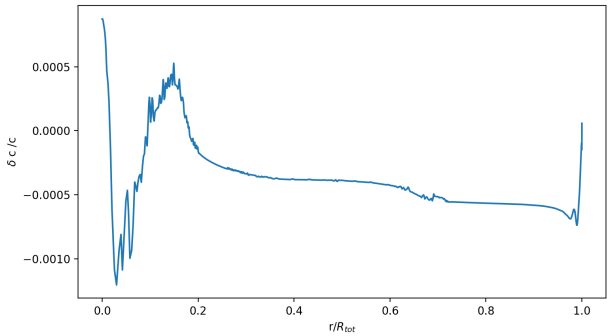

Fig. 4. Evolution of the sound speed, c, profile relative difference between the ICSM and a relaxed model with the same composition.

This is currently under investigation as it could have some importance when looking at the Sun because of the strong

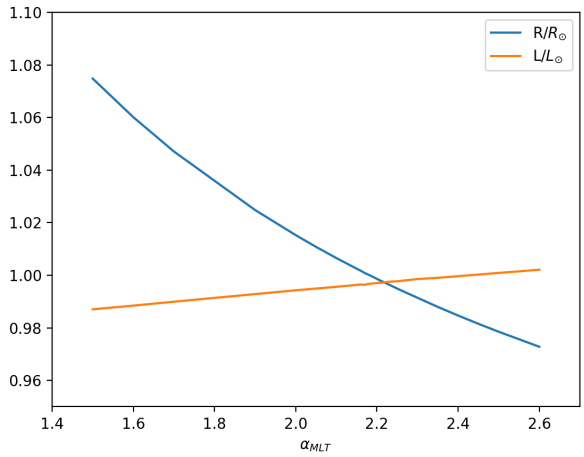

Fig. 5. Evolution of radius, R, and luminosity, L, with the mixing length parameter $\alpha_{\rm MLT}$ for the ICSM.

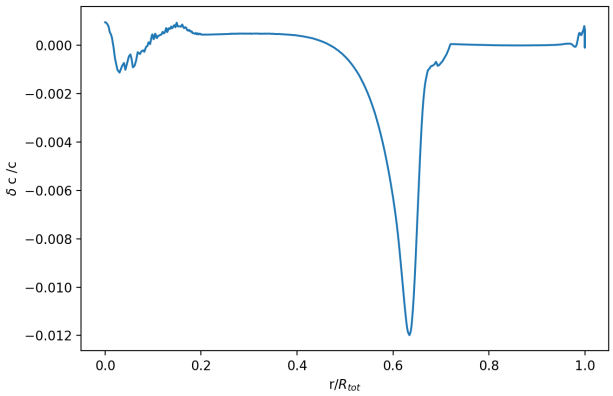

Fig. 6. Evolution of the sound speed, c, profile relative difference between the ICSM and an optimized model with perturbed composition.

observational constraints in that case. However, the resulting relative differences are very small, i.e. less than 0.20% and 0.15% for the X and c profiles, respectively. Thus this will not be an important issue when studying all others stars as the uncertainties on observed quantities are larger.

With no perturbation to initial model, we also tried to determined the effect of varying the mixing length parameter $\alpha_{\rm MLT}$. This can be visualized on Fig. 5. We can clearly see that there is an important impact on both radius and luminosity. Radius is decreasing and luminosity increasing with $\alpha_{\rm MLT}$. Also it appears that there is an optimal value for $\alpha_{\rm MLT}$ that gives values of R and L both very close to the solar values. This value is $\alpha_{\rm MLT} \simeq 2.2$, which is also the result of the solar calibration.

4.2. Simple Optimizer

In order to test the feasibility of our idea, we have first done a test with a simple Nelder-Mead optimizer using only 3 parameters: $\alpha_{\rm MLT}$ and the first knot in the radiative zone, just under the convective boundary for the X and Y profile, $X_{\rm CB}$ and $Y_{\rm CB}$. As an initial guess for the parameters we used the values from the ICSM. The objective function of the optimizer is the same as Eq. (7). The optimization run outputs for $\alpha_{\rm MLT}$, $X_{\rm CB}$ and $Y_{\rm CB}$ a change of $\sim -5\%$, $\sim 0\%$ and $\sim -10\%$ compared to their initial respective values. The impact on the sound speed profile is presented on Fig. 6.

The resulting sound speed profile exhibits a significant difference at the location where the composition is perturbed. The sound speed is increased by approximately 1.2% at maximum. This is promising as when comparing models to observations, there is a well-known discrepancy at this location. Generally, SSM present a sound speed that is smaller than the observed value (see for example Fig. 39 of Christensen-Dalsgaard 2021).

The objective of our project is to use constraints from helio- and asteroseismology to obtain realistic models of stellar structures. Then, the echelle diagrams presented on Fig. 7 compared the modelled frequencies with the observed ones in the range 1 mHz to 4mHz and for harmonic degrees $\ell = 0, 1, 2$ and 3. On these diagrams the frequencies are represented modulo $\Delta\nu$, as given by (Christensen-Dalsgaard 2014)

$$\nu_{n,\ell} = \nu_0 + k\Delta\nu + \tilde{\nu}_{n,\ell}, \tag{9}$$

with ν_0 a reference frequency and k an integer such that $\tilde{\nu}_{n,\ell}$ is between 0 and $\Delta\nu$. The large frequency separation, $\Delta\nu$, is the difference in frequency between two modes of the same degree and of consecutive radial order

$$\Delta\nu_\ell = \nu_{n+1,\ell} - \nu_{n,\ell}. \tag{10}$$

The modelled frequencies are computed using the oscillations code GYRE (version 6.0) (Townsend & Teitler 2013; Townsend et al. 2018). First we can notice the effect of correcting the modelled frequencies using the the surface term correction described in Section 3.2. The modelled frequencies are represented with blue dots and the corrected ones with orange dots. As expected, the effect of the correction increases with frequencies. The agreement with helioseismic data is indeed better after correction.

Next, comparing the corrected modelled frequencies for the ICSM (left panel) and the optimized model (right panel), the latter shows a better agreement with observations. This suggests that the optimized structure could be a more realistic representation of the actual structure of the Sun. However, this study needs to be continued in order to confirm or not such suggestion. Indeed, even if we obtain a better agreement for sound speed and oscillations frequencies, the luminosity, $L = 0.993834 L_\odot$, of the optimized model agreed a little bit less with the observed value than the ICSM, $L = 0.999999 L_\odot$. This can appear like a relatively small difference, but as investigating the details of the theory of stellar structure and evolution, we would like to be as precise as possible.

Moreover, the main problem with a simple optimizer like the Nelder-Mead used here, is that it only gives one possible solution to the problem. What we have here is a local minimum and we would like to obtain the global minimum. It is for this reason that we are implementing an MCMC method to get the full range of stellar structures that are supported by the observational data. This is undergoing work but some preliminary results are presented in the next section.

4.3. Preliminary results with the MCMC

This is ongoing work and the results will be published later.

5. Conclusions

This study presents an innovative method for stellar inversion based on a non-linear approach.

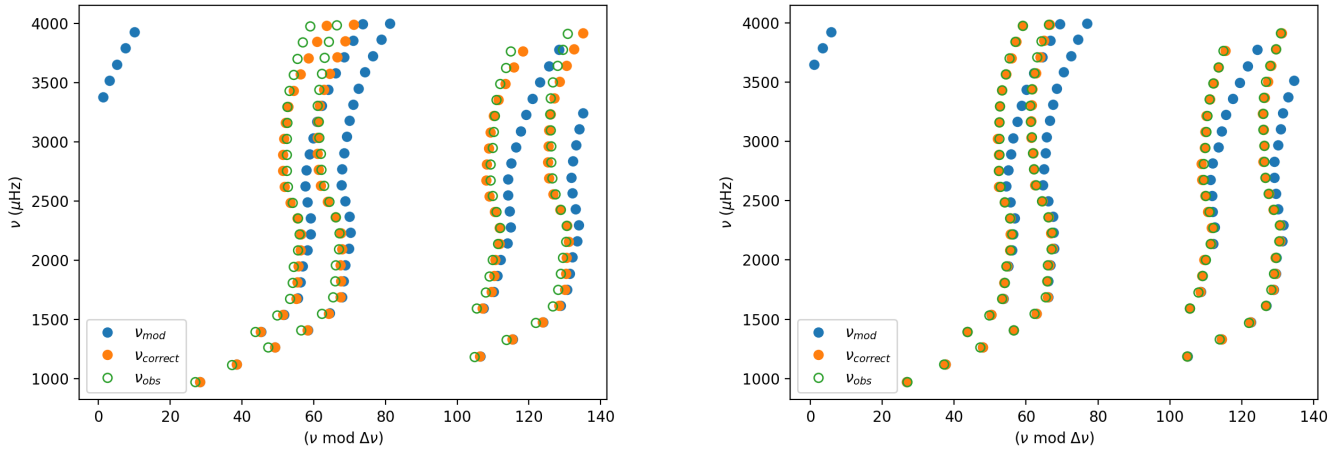

Fig. 7. Echelle diagrams comparing the modeled (blue filled circle) and corrected (orange filled circles) frequencies of ICSM (left panel) and an optimized model (right panel), with observations (green empty circles) of harmonic degrees $\ell = 0, 1, 2$ and 3.

Acknowledgements. This work was initiated during the 2021 Kavli Summer Program in Astrophysics, hosted by the Max Planck Institute for Solar System Research, and funded by the Kavli Foundation.

References

Asplund, M., Grevesse, N., Sauval, A. J., & Scott, P. 2009, ARA&A, 47, 481
Auvergne, M., Bodin, P., Boisnard, L., et al. 2009, A&A, 506, 411
Bahcall, J. N., Basu, S., Pinsonneault, M., & Serenelli, A. M. 2005, ApJ, 618, 1049
Ball, W. H. & Gizon, L. 2014, A&A, 568, A123
Basu, S. 2016, Living Reviews in Solar Physics, 13, 2
Bellinger, E. P., Angelou, G. C., Hekker, S., et al. 2016, ApJ, 830, 31
Bellinger, E. P., Basu, S., & Hekker, S. 2020, Astrophysics and Space Science Proceedings, 57, 171
Bellinger, E. P., Basu, S., Hekker, S., & Ball, W. H. 2017, ApJ, 851, 80
Bellinger, E. P., Basu, S., Hekker, S., Christensen-Dalsgaard, J., & Ball, W. H. 2021, ApJ, 915, 100
Borucki, W. J., Koch, D., Basri, G., et al. 2010, Science, 327, 977
Brooks, S., Gelman, A., Jones, G., & Meng, X. 2011, Handbook of Markov Chain Monte Carlo (Chapman and Hall/CRC)
Broomhall, A.-M., Chaplin, W. J., Davies, G. R., et al. 2009, Monthly Notices of the Royal Astronomical Society: Letters, 396, L100
Christensen-Dalsgaard, J. 2014, Lecture notes on stellar oscillations (Aarhus University)
Christensen-Dalsgaard, J. 2021, Living Reviews in Solar Physics, 18, 2
Christensen-Dalsgaard, J., Proffitt, C. R., & Thompson, M. J. 1993, ApJ, 403, L75
Davies, G. R., Broomhall, A. M., Chaplin, W. J., Elsworth, Y., & Hale, S. J. 2014, MNRAS, 439, 2025
Davies, G. R., Chaplin, W. J., Farr, W. M., et al. 2015, MNRAS, 446, 2959
Eilers, P. H. C. & Marx, B. D. 1996, Statistical Science, 11, 89
Foreman-Mackey, D., Hogg, D. W., Lang, D., & Goodman, J. 2013, PASP, 125, 306
Gough, D. 1990, in Progress of Seismology of the Sun and Stars, ed. Y. Osaki & H. Shibahashi (Berlin, Heidelberg: Springer Berlin Heidelberg), 281–318
Grevesse, N. & Sauval, A. J. 1998, Space Sci. Rev., 85, 161
Gruberbauer, M., Guenther, D. B., & Kallinger, T. 2012, ApJ, 749, 109
Hale, S. J., Howe, R., Chaplin, W. J., Davies, G. R., & Elsworth, Y. P. 2016, Sol. Phys., 291, 1
Kjeldsen, H., Bedding, T. R., & Christensen-Dalsgaard, J. 2008, ApJ, 683, L175
Ong, J. M. J., Basu, S., & McKeever, J. M. 2021, ApJ, 906, 54
Paxton, B., Bildsten, L., Dotter, A., et al. 2011, ApJS, 192, 3
Paxton, B., Cantiello, M., Arras, P., et al. 2013, ApJS, 208, 4
Paxton, B., Marchant, P., Schwab, J., et al. 2015, ApJS, 220, 15
Paxton, B., Schwab, J., Bauer, E. B., et al. 2018, ApJS, 234, 34
Paxton, B., Smolec, R., Schwab, J., et al. 2019, ApJS, 243, 10
Ramírez, I., Meléndez, J., & Asplund, M. 2009, A&A, 508, L17
Rauer, H., Catala, C., Aerts, C., et al. 2014, Experimental Astronomy, 38, 249
Ricker, G. R., Winn, J. N., Vanderspek, R., et al. 2014, Journal of Astronomical Telescopes, Instruments, and Systems, 1, 1
Roxburgh, I. & Vorontsov, S. 2003, Ap&SS, 284, 187
Schmitt, J. R. & Basu, S. 2015, ApJ, 808, 123
Serenelli, A. 2016, European Physical Journal A, 52, 78
Silva Aguirre, V., Lund, M. N., Antia, H. M., et al. 2017, ApJ, 835, 173
Townsend, R. H. D., Goldstein, J., & Zweibel, E. G. 2018, MNRAS, 475, 879
Townsend, R. H. D. & Teitler, S. A. 2013, MNRAS, 435, 3406
White, T. R., Huber, D., Maestro, V., et al. 2013, MNRAS, 433, 1262